# HYBRID FD-FD ANALYSIS OF CROSSING WAVEGUIDES BY EXPLOITING BOTH THE PLUS AND THE CROSS STRUCTURAL SYMMETRY

## H.-W. Chang, Y.-H. Wu, and W.-C. Cheng

Institute of Electro-optical Engineering and Department of Photonics
National Sun Yat-sen University
Kaohsiung 80424, Taiwan

**Abstract**—We propose a hybrid finite-difference frequency-domain method to study the perpendicular crossing waveguide, dielectric and microwave, TE and TM modes, by exploiting built-in structural symmetries in these waveguide devices. In the plus (+) symmetry model, the complete solution is obtained by solving two rectangular-shaped quarter structures each with two transparent boundaries and two symmetry boundaries. For the cross (×) symmetry model, solutions of four triangular-shaped quarter structures are needed but each with only one transparent boundary. Numerical results are verified by comparison between these two models and with the power conservation test. We show the total and the fundamental-mode, coupling coefficients of the reflected, cross and through power in the crossing waveguide as functions of the normalized frequency.

## 1. INTRODUCTION

As the complexity of the planar lightwave circuit increases, the optical interconnect problem becomes more and more important [1–3]. It is necessary to characterize the photonic crossings composed of the dielectric waveguides, especially in silicon on insulator (SOI) photonic waveguide devices made with high-contrast refractive index materials, for increasing the interconnect capability.

In recent years the growing impact of photonic interconnects has attracted many publications [4–16]. It was reported that the right angle crossings have smaller crosstalk than shallow angle ones [4]. The power coupling coefficient may approach unity by a proper modification on the shape of the intersection part [11]. In this paper, we focus

---

Corresponding author: H.-W. Chang (hchang@faculty.nsysu.edu.tw).

on the discussion of the right angle crossing. Low-loss and low-crosstalk crossing makes the routing of complex photonic circuits easier than the electronic circuits. In order to improve the throughput and to lower the crosstalk, manuscripts report different modifications of the simple crossing structure including the multimode interference (MMI) structure, resonant cavity and elliptical or parabolic mode expanders. The exact calculation of the loss and crosstalk as function of the wavelength is of great importance for these designs of dielectric crossings. Numerical techniques for the study of the crossings include the finite-difference time-domain (FD-TD) [6, 7, 10, 12], the beam propagation method (BPM) [4, 8, 16], the mode-matching method [13], the finite element method (FEM) [14], the method of line [9] and the coupled-mode theory [16], etc. Furthermore, on SOI based integrated circuits with a high index contrast between the silicon core and the silica cladding, the optical wave of a small cross-sectional intersection would produce a larger crosstalk and more reflections at the junction. The horizontal and vertical traveling fields of two crossing waveguides are tightly coupled in the vicinity of the intersection. These quadridirectional wave fields are so complex that it is difficult to analyze them with rigorous methods such as the mode matching methods and the coupled transverse-mode integral equation CTMIE methods [17, 18]. Many such mode-based methods adopt the PECAM (perfect electric conductor approximation) [19] approximation which confines the wave fields to propagate only horizontally. Although, it is possible to modify the mode matching method to obtain a quadridirectional eigenmode expansion scheme [20] for crossing waveguides, this highly accurate method is far too complex to be practical for an arbitrary crossing profile. The general PML boundary conditions are often combined with PECAM schemes but it is not suitable for the waveguide crossing due to the strong evanescent waves in the cladding region of guiding modes [21–23]. Recently, we developed the layer-mode transparent boundary condition (LM-TBC) [24] which can absorb/transmit both the guided modes, discretized radiation modes and even the evanescent modes in both crossing waveguides. We seek to combine LM-TBC with the hybrid frequency-domain finite-difference (FD-FD) method to study dielectric waveguide crossings.

## 2. HYBRID FD-FD METHOD

In this paper, we propose to conduct a two-dimensional ($x$-$z$ plane) hybrid FD-FD study of the perpendicular waveguide crossing as shown in Figure 1(a). To accurately simulate quadridirectional wave
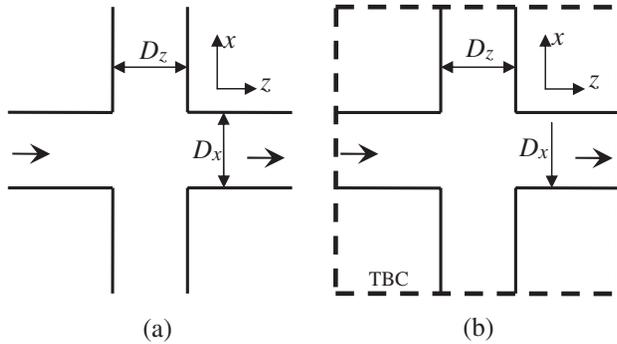
**Figure 1.** (a) The open perpendicular microwave waveguide crossing in a $z$-$x$ coordinate system. (b) The computational domain is surrounded with numerically transparent borderlines indicated by four dashed lines.

fields in the waveguide intersection by a general FD-FD method we need to enclose the computational domain with transparent boundary conditions (TBC) on all four borderlines shown as the dash lines in Figure 1(b). The TBC is crucial for a successful crossing analysis. Because a "good" TBC not only reduces the size of the computational domain but also guarantees the accuracy of computed scattered wave fields. Let $D_x$ and $D_z$ be the microwave waveguide (or dielectric waveguide core) thickness of the horizontal and vertical waveguide respectively and $\lambda$ be the wavelength of the incident field which we assume to be the fundamental mode coming from the left side.

We can further reduce FD-FD computational domain by taking the advantage of the symmetries in the device. The plus (+) symmetry shown in Figure 2(a) is always there for a perpendicular crossing. When both waveguides are identical in shape we have also the cross (×) symmetry as shown in Figure 2(b). In 2009, we reported the simulation of a dielectric waveguide crossing using a hybrid FD-FD method and by exploiting the cross symmetry [25]. When the plus/cross symmetry is applied to a crossing waveguide, the original problem can be broken down into two/four subproblems each being one quarter of the full size. The sub-solutions are then reassembled to form the full solution. In doing so we reduce both CPU time and memory requirement of the full problem and in the case of cross symmetry we also avoid the difficulty of implementing two TBCs on the top and left boundaries of Figure 2(a).

In the plus symmetry, we have both the horizontal and the vertical axes as symmetric lines. The two lines divide the device into four parts.

We choose the second quadrant as our reduced computational region. Among the four boundaries, the right and the bottom boundaries are PECW/PMCWs (perfect electric/magnetic conducting walls). The left and the top boundaries are transparent boundaries. In the open dielectric waveguide case locations of TBCs are placed far enough to reduce side effects due to the PECW/PMCW corner, but not too far to keep the computational requirement in check. Our LM-TBC is used on the left boundary to simultaneous launch the incident field and to allow the reflected wave fields to pass through this boundary. As for the top TBC, we are not able to directly apply LM-TBC due to the limitation of our matrix solver which uses a modified Thomas method [26, 27] to perform the Gaussian elimination. The block tri-diagonal structure of the resulting matrix is destroyed by the top LM-TBC that uses a full matrix to connect the unknowns in the top row of Figure 3(a). As a result, we are forced to simplify the top TBC by using the fundamental-mode approximation for the upward traveling waves. Nevertheless, this one-term TBC approach demonstrates a four digit precision in our numerical results for microwave cases with just one even mode and perhaps one odd mode. It fails to deliver a good solution in the dielectric case where there are many more cladding modes. For those cases where the plus symmetry fail we will consider the cross symmetry.

In the cross symmetry shown in Figure 2(b), we have two $\pm 45°$ symmetric lines perpendicular to each other. We choose the left triangular area as our computational domain. In reality we place the triangular area into an enclosing rectangular domain so that our existing matrix solver will continue to work. This model



(a)                                          (b)
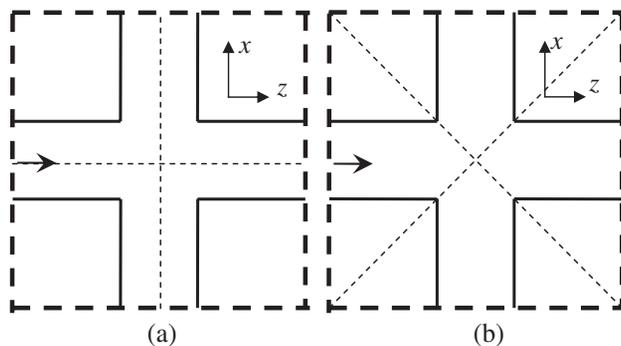
**Figure 2.** Schematic illustration of dual two-fold symmetries in a perpendicular crossing waveguide. (a) Plus (+) symmetry on $x$ and $z$ axes. (b) Cross (×) symmetry on two diagonal axes.

includes one LM-TBC and two symmetric lines each with an equivalent PECW/PMCW pair. By using the combination of PEC/PMC walls, we reduce the original full problem to four subproblems requiring less computing resources. We shall compute the microwave and dielectric waveguide crossings and compare computed power coefficients between plus and cross symmetry.
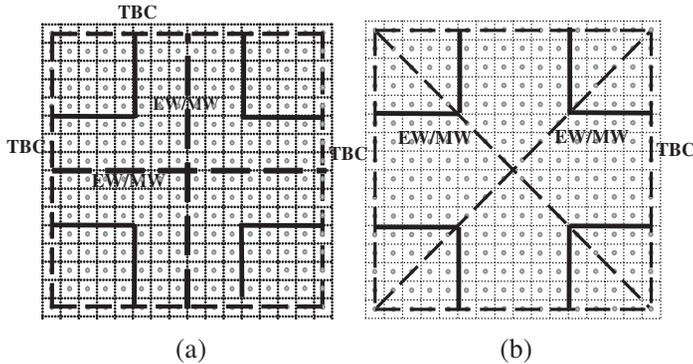


**Figure 3.** FD-FD grid layouts for the plus symmetry (a) and for the cross symmetry (b).

## 3. BUILDING TWO SYMMETRY MODELS

### 3.1. FD Approximation of Helmholtz Equation

We write down the two-dimensional Helmholtz equation for TE and TM modes as the following:

$$
\begin{aligned}
&\frac{\partial^2}{\partial x^2}E_y + \frac{\partial^2}{\partial z^2}E_y + n^2(x,z)k_0^2 E_y(x,z) = 0, \\
&\frac{\partial}{\partial x}\left[\frac{1}{n^2(x,z)}\frac{\partial}{\partial x}H_y\right] + \frac{\partial}{\partial z}\left[\frac{1}{n^2(x,z)}\frac{\partial}{\partial z}H_y\right] + k_0^2 H_y(x,z) = 0.
\end{aligned}
\tag{1}
$$

The detailed hybrid FD-FD formulations can be found in reference [24] where the entire problem is divided into one FD-FD region for the central structure and one to several analytical regions for waveguide structures. Here we derive the corresponding FD-FD coefficients for unknowns near the PECW/PMCW boundaries. In the following derivation, superscript 'e' denotes TE mode with the $E_y$ component and 'h' stands for the TM mode with $H_y$ component. Subscripts $c, u, d, \ell, r$ denotes center, up, down, left and right respectively. Applying the second-order accurate FD approximation to

Equation (1), we obtain the discrete 2-D Helmholtz equation for field $u_c$ which is a five-point formula connecting itself to the four neighboring points $u_u, u_d, u_\ell, u_r$. We have

$$c_u^e u_u + c_d^e u_d + c_\ell^e u_\ell + c_r^e u_r + c_c^e u_c = 0,$$
$$c_u^h u_u + c_d^h u_d + c_\ell^h u_\ell + c_r^h u_r + c_c^h u_c = 0, \tag{2}$$

where the coefficients are given by

$$c_u^e = c_d^e = 1/\Delta x^2, \quad c_\ell^e = c_r^e = 1/\Delta z^2,$$
$$c_c^e = \overline{n_c^2} k_0^2 - (c_u^e + c_d^e + c_\ell^e + c_r^e),$$
$$c_u^h = \overline{\frac{1}{n_u^2}} \frac{1}{\Delta x^2}, \ c_d^h = \overline{\frac{1}{n_d^2}} \frac{1}{\Delta x^2}, \ c_\ell^h = \overline{\frac{1}{n_\ell^2}} \frac{1}{\Delta z^2}, \ c_r^h = \overline{\frac{1}{n_r^2}} \frac{1}{\Delta z^2},$$
$$c_c^h = k_0^2 - \left(c_u^h + c_d^h + c_\ell^h + c_r^h\right). \tag{3}$$

Here $k_0$ is the wave number in vacuum. $\overline{n_c^2}$ is given by the areal average of $n^2(x, z)$ centered around $u_c$ over a grid cell area $\Delta x \cdot \Delta z$. TM case requires $\overline{1/n_p^2}$ average which is defined as the areal average of $1/n_p^2(x, z)$ centered at $u_p$. When $p = u, d, \ell, r$, the center of the integration point is located half a grid up, down, left and right from $u_c$ respectively. TE and TM FD coefficients are identical except for those points laid within one grid away from boundaries between two materials. Figure 3 shows the complete grid layout for both the plus and the cross symmetry cases. All grid points are located on the center of each grid cell. For points bordering a PECW (PMCW) or a symmetry wall, they are placed half a grid inside these walls. The exceptions are the two PEC/PMC walls of the 45 degree symmetric lines. The grid points are on these lines. In LM-TBC the interface between the FD-FD domain and the analytical domain also passes through the grid points which are shared by the two domains. The above setup of the grid layout is convenient for the boundary conditions and the material averaging scheme in our numerical analysis.

## 3.2. Boundary Conditions for the Plus-symmetry Model

Figure 4 presents the grid layout and the boundary conditions for the plussymmetry model. In our numerical simulation we assume that $D_x = D_z$, $\Delta x = \Delta z$ and there are total $N$ field points along $x$ and $z$ axis. Referring to Figure 4, to the left is the LM-TBC and to the right a PECW or PMCW. The boundary condition of the bottom wall is treated with even symmetry for the fundamental incident mode and with odd symmetry for other higher anti-symmetric modes Depending on the particular symmetry, we have $u_d = \pm u_c$ due to the fact that the PEC/PMC wall is located exactly half way in between. Equation (2)

at the bottom boundary can be rewritten as

$$c_u^e u_u + c_\ell^e u_\ell + c_r^e u_r + (c_c^e \pm c_d^e) u_c = 0,$$
$$c_u^h u_u + c_\ell^h u_\ell + c_r^h u_r + (c_c^h \pm c_d^h) u_c = 0. \tag{4}$$

The coefficients for points near the bottom boundary are

$$(c_c^e)_{\text{new}} = (c_c^e \pm c_d^e), \quad (c_d^e)_{\text{new}} = 0,$$
$$\left(c_c^h\right)_{\text{new}} = \left(c_c^h \pm c_d^h\right), \quad \left(c_d^h\right)_{\text{new}} = 0. \tag{5}$$

Here the plus/minus sign is taken depending on the even/odd symmetry of the boundary condition. Similarly, the coefficients for points near the right boundary are given by

$$(c_c^e)_{\text{new}} = (c_c^e \pm c_r^e), \quad (c_r^e)_{\text{new}} = 0,$$
$$\left(c_c^h\right)_{\text{new}} = \left(c_c^h \pm c_r^h\right), \quad \left(c_r^h\right)_{\text{new}} = 0. \tag{6}$$

As discussed earlier, our direct FD-FD solver prevents the application of full LM-TBC for the top boundary; we assume that the outgoing waves are dominated by the fundamental mode. Thus, for all $m = 1, \ldots, N$, outside field point $u_{N+1,m}$ can be related to inside point $u_{N,m}$ by the following equation:

$$u_{N_x+1,m} = u_{N_x,m} \cdot \exp\left(-j\beta_1^x \cdot \Delta x\right), \tag{7}$$

where $\beta_1^x$ is the propagation constant of the fundamental mode of the vertical waveguide, $x = e/h$ is the type of polarization. The resulting coefficients for these grids on the top row are given by

$$(c_c^x)_{\text{new}} = c_c^x + c_u^x \cdot \exp\left(-j\beta_1^x \cdot \Delta x\right), \quad (c_u^x)_{\text{new}} = 0, \quad x = e, h. \tag{8}$$

For microwave crossing waveguides we need to take care of the two PECWs (part of the waveguide structure, depicted by solid lines in Figure 4) inside the computational domain. The coefficients for inside points bordering the plate are rewritten as

$$(c_c^e)_{\text{new}} = c_c^e - c_x^e, \quad (c_x^e)_{\text{new}} = 0, \quad x = r, d,$$
$$\left(c_c^h\right)_{\text{new}} = c_c^h + c_x^h, \quad \left(c_x^h\right)_{\text{new}} = 0, \quad x = r, d. \tag{9}$$

Finally, for microwave cases, we assign a simple equation such as $u_{i,j} = 0$ for points (hollow points of Figure 4) inside the computational domain but outside these two PECWs so they will be decoupled from points inside the crossing waveguide. The LM-TBC equations together with Equations (2)–(9) form the self-consistent discretized Helmholtz equation for a crossing waveguide with the plus-symmetry model. The FD-FD solution for points on the left/top boundary will provide us
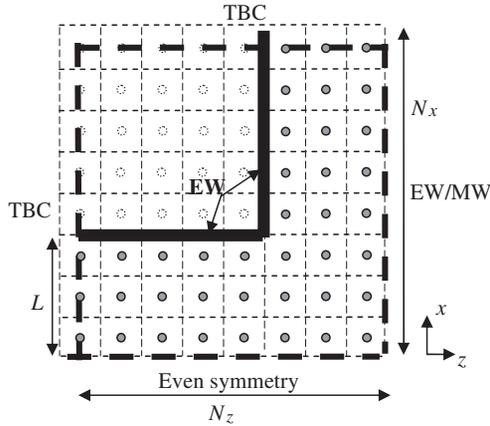
**Figure 4.** The grid layout and the boundary conditions for the quarter-size subproblem in the plus-symmetry model.

with the reflection/transmission coefficient vectors in the analytical regions [24].

The final FD-FD equations for all field points inside the computational domain form an $N^2 \times N^2$ sparse matrix. With the one-mode TBC approximation for the top boundary, this matrix is in a block tri-diagonal form with its diagonal blocks as $N \times N$ tri-diagonal matrices and off diagonal blocks as $N \times N$ diagonal matrices. We solve this matrix equation by the direct method using the Gaussian elimination or LU factorization. With a modified Thomas method, we are able to obtain a solution with up to a quarter million unknowns under ten CPU minutes on a PC using Matlab. The complete crossing field $E_y(x, z)$ or $H_y(x, z)$ can be constructed from the even sub-solution $F^e$ and the odd sub-solution $F^o$ of Figure 4. There are two ports — an input $F_i^e, F_i^o$ and an output port $F_0^e, F_0^o$ in both solutions. They are symmetrical with respect to $y$-$z$ plane. After we obtain the even and odd results of the field in the second quadrant, we then extend the field to other quadrants by flipping the field image, first across the $x$ axis with no sign change, and then across the $z$ axis with a proper sign change. Thus, $F_i^e/F_i^o$ is on the left half of Figure 3(a) and $F_0^e/F_0^o$ on the right half of Figure 3(a). We will arrive at two full solutions shown in Figures 5. From the average of these two full solutions, we obtain the complete solution of a crossing waveguide excited by an even waveguide mode incident from the left (port No. 1). The reflection coefficient ($R_1$), cross transmission coefficients for port 2, 4 ($T_2, T_4$)

(a) Even case                    (b) Odd case
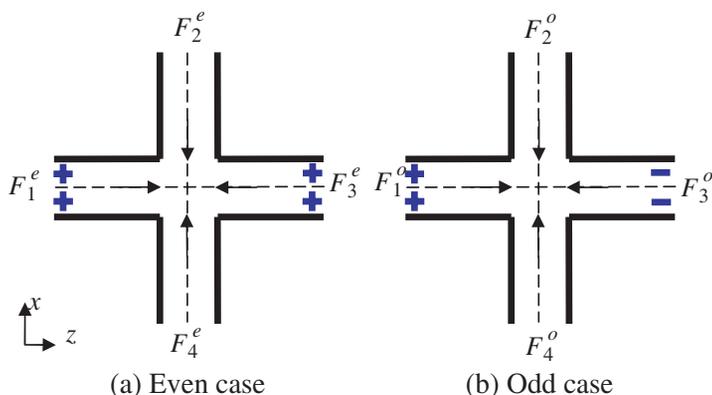
**Figure 5.** Illustration of constructing the complete solution of the plus-symmetry model. The equivalent boundary conditions can be realized by sending an (even) incident field from the left waveguide and also from the right waveguide with or without a sign change. This would make $z$-axis even and the $x$-axis even (a) or odd (b) note that the average of (a) and (b) leads to the original full solution of a crossing waveguide in Figure 2(a).

and through transmission coefficients for port 3 ($T_3$) are given by:

$$
\begin{aligned}
R_1 &= \frac{R^e + R^o}{2}, & T_2 &= \frac{T^e + T^o}{2}, \\
T_3 &= \frac{R^e - R^o}{2}, & T_4 &= \frac{T^e + T^o}{2}.
\end{aligned}
\tag{10}
$$

Here $R^e/R^o$ and $T^e/T^o$ is the reflection and transmission coefficients of the even/odd sub-solution respectively. Port three is the through waveguide and ports two and four are the cross waveguides.

### 3.3. Boundary Conditions for the Cross-symmetry Model

Figure 6 illustrates the grid layout and boundary conditions for the crosssymmetry model. We divide the grids in the $z$ direction into two regions. The first one consists of a short section of a parallel-plate waveguide ($N_{z1} \times N_x$ grids) is acting as the buffer region between the analytic domain and FD domain. It has two PECWs on the top and bottom borders and a TBC on the left boundary. The second region is made of one quarter of the overlapped waveguides ($N_{z2} \times N_x$ grids). For this region, there are four combinations of PECW and PMCW along the two diagonal axes.
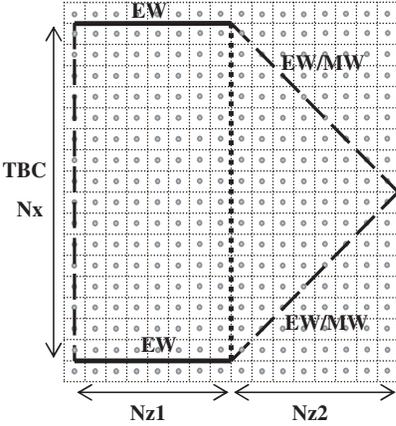
**Figure 6.** The grid layout and boundary conditions for the quarter-size subproblem in the cross-symmetry model.
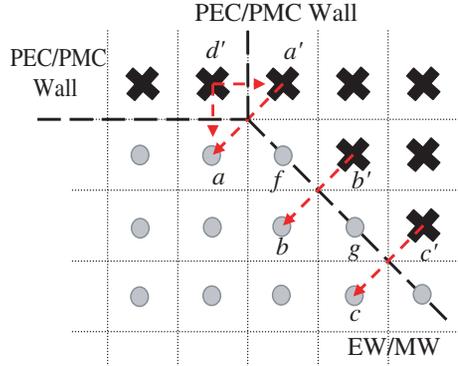
**Figure 7.** The grid layout around the waveguide corner for the cross-symmetry model.

The PECW boundary conditions for the parallel-plate waveguide section are handled in the same way as in Equation (9) for the plus-symmetry model. However, we need to take extra care to modify FD coefficients for those grids on the symmetry lines, around the corner and on the tip of the quarter structure in Figure 6. In Figure 7, point $g$ represents a regular point on one of the symmetry line whereas point $f$ is another point but lies near the waveguide corner. Each regular point has four neighbors, points $b'$, $c'$ outside the substructure and points $b$, $c$ inside the substructure. Field at point $b'(c')$ is equal or opposite to field at $b(c)$ depending on symmetry type of the line dividing them. For the central point $g$ we need to transfer the FD coefficients associated with outside points to their corresponding inside points as the following

$$
\begin{aligned}
(c_\ell^x)_{\text{new}} &= c_\ell^x \pm c_u^x, \quad (c_u^x)_{\text{new}} = 0, \quad x = e, h, \\
(c_d^x)_{\text{new}} &= c_d^x \pm c_r^x, \quad (c_r^x)_{\text{new}} = 0, \quad x = e, h.
\end{aligned}
\tag{11}
$$

Like Equations (5)–(6), the plus/minus sign is taken depending on the even/odd symmetry of the diagonal lines. For point $f$ Equation (11) is only an approximation since the field at point $a'$ does not have a simple mirror point (point $a$) due to the nearby corner. We have found the additional error associated with this corner point can be reduced with the increase of the $N_{z2}$ parameter.

Next, we consider FD coefficients for points near the tip where the two symmetry lines meet. A blow-up version of Figure 6 is shown
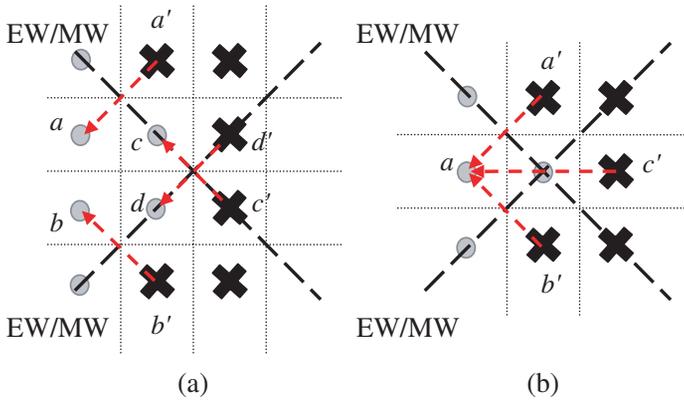
**Figure 8.** The grid points around the sub-structure tip for the cross-symmetry model. (a) For an even $N_x$ no points on the tip. (b) For an odd $N_x$ one grid point on the tip.

in Figures 8 where we consider both the even $N_{z2}$ and the odd $N_{z2}$ cases. In either case $N_{z2} = N_x$ is assumed. Figure 8(a) shows two regular points which are close to but not on the tip. Point $c$ and $d$ follow the rules of Equation (11). The case with an odd $N_x$ is shown in Figure 8(b). It has a grid point located on the tip. The fields at grids $a'$, $b'$, $c'$ can be referred to the value at point $a$ by symmetry. The field at this point is nonzero only when both symmetry lines are even. And we need to modify the coefficients in Equation (2) according to the following rules

$$(c_\ell^x)_{\text{new}} = (c_\ell^x + c_u^x + c_r^x + c_d^x), \quad x = e, h,$$
$$(c_r^x)_{\text{new}} = (c_u^x)_{\text{new}} = (c_d^x)_{\text{new}} = 0. \tag{12}$$

The other three combinations of this "$x$" symmetry pair imply a null field for point on the tip and the following rules apply

$$(c_r^x)_{\text{new}} = (c_u^x)_{\text{new}} = (c_d^x)_{\text{new}} = (c_\ell^x)_{\text{new}} = 0.$$
$$(c_c^x)_{\text{new}} = 1. \tag{13}$$

The procedure for obtaining full FD-FD simulation results of cross-symmetry model is similar to that of the plus-symmetry model. For cross symmetry there are four independent simulation of the sub-structure of Figure 6 with a pair of symmetry denoted by a subscript of MM, EM, ME and EE. The first letter represents the PEC/PMC wall (EW/MW for short) on the upper right border and the second letter for the lower right boundary. Furthermore there are only three independent calculations. We observe that the EW/MW and the
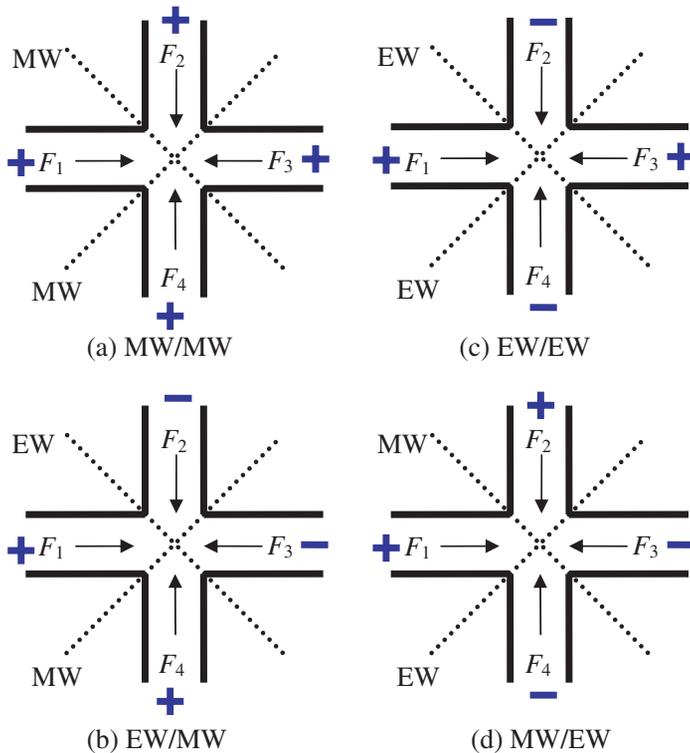
**Figure 9.** Illustration of constructing the complete solution of the cross-symmetry model. This cross symmetry can be realized by sending identical incident fields toward the device center from all four waveguide ports. For the TE polarization each specific sign arrangement of the incident field will generate equivalent boundary conditions of (a) MW/MW, (b) EW/MW, (c) EW/EW and (d) MW/EW on the two diagonal lines Note that the average of (a), (b), (c) and (d) leads to the original full solution to a crossing waveguide as in Figure 2(b).

MW/EW cases produce results which are mirror (on the $y$-$z$ plane) images of each other. Figure 9 illustrates ways to form field with two-fold diagonal symmetries by launching an identical mode with proper sign toward the crossing zone from all four waveguides. These four fields are denoted by $U_{\mathrm{MM}}, U_{\mathrm{EE}}, U_{\mathrm{EM}}, U_{\mathrm{ME}}$. We see that one quarter sum of all four simulations will produce no incident wave field from the top, down and right waveguide but just once incident field coming from the left waveguide. Denoting the reflection coefficient of the Figure 6

waveguide by $R_{\mathrm{MM}}, R_{\mathrm{EE}}, R_{\mathrm{EM}}, R_{\mathrm{ME}}$, we obtain the reflection cross and through transmission coefficients for port 1 to 4 as the following equation:

$$R_1 = \frac{R_{\mathrm{MM}} + R_{\mathrm{EE}} + R_{\mathrm{EM}} + R_{\mathrm{ME}}}{4}, \quad T_2 = \frac{R_{\mathrm{MM}} - R_{\mathrm{EE}} - R_{\mathrm{EM}} + R_{\mathrm{ME}}}{4},$$
$$T_3 = \frac{R_{\mathrm{MM}} + R_{\mathrm{EE}} - R_{\mathrm{EM}} - R_{\mathrm{ME}}}{4}, \quad T_4 = \frac{R_{\mathrm{MM}} - R_{\mathrm{EE}} + R_{\mathrm{EM}} - R_{\mathrm{ME}}}{4}. \tag{14}$$

## 4. RESULTS AND DISCUSSION

In this section, we report the numerical results on the wave fields and power reflection, through and cross transmission coefficients of microwave and dielectric crossing waveguides for both TE and TM cases. Detailed reports on the effect of modeling parameters such as discretization density, the PECAM corner side effects due to LM-TBC are given in one of the author's thesis [26].

### 4.1. Two-Dimensional Field Plots

For the analysis of the microwave waveguide crossing, we define a parameter $B$ as the normalized frequency which is defined as

$$B = \frac{2D}{\lambda}. \tag{15}$$

Here $D$ is the microwave waveguide width. The normalized frequency is a dimensionless quantity and is the key to constructing the universal curves in this paper. The TE field distributions of plus- and cross-symmetry models are shown in Figures 10 and 11 for $B = 1.6$
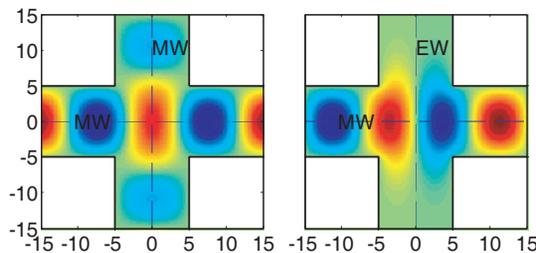


**Figure 10.** Expanded $E_y(x, z)$ field distributions of the plus-symmetry model for the microwave crossing waveguide with a normalized frequency $B = 1.6$. The even symmetry is on the left and the odd on the right. These are standing wave with only real parts.
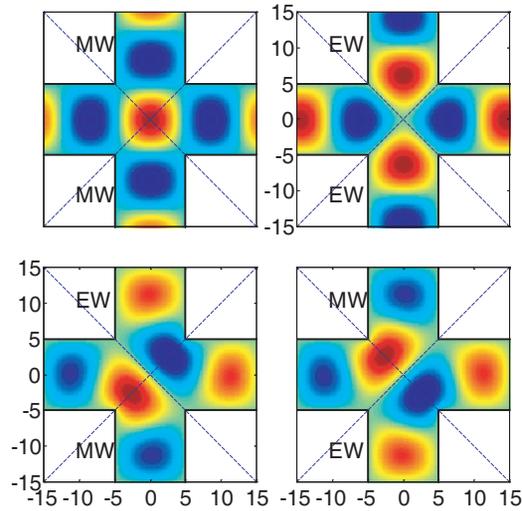
**Figure 11.** Expanded $E_y(x, z)$ field distributions of the cross-symmetry model for the microwave crossing waveguide with a normalized frequency $B = 1.6$. Note that the EW/MW case is the anti-mirror version of the MW/EW case. These are standing wave with only real parts.
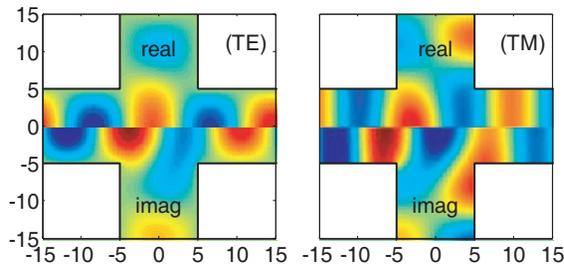


**Figure 12.** Complete TE and TM field distributions of a microwave crossing waveguide constructed from averages of Figures 10–11. Propagating wave fields are made visible with the real part on the upper halves and the imaginary part on the bottom halves. The difference between the plus- and the cross-symmetry models is too small to show.

corresponding to a microwave frequency of $2.45\,\text{GHz}$ ($\lambda = 12.5$ cm) and a waveguide width of 10 cm. Figure 10 shows the plus-symmetric cases after flipping the image with respect to the $x$ and $z$ axis. Complete microwave crossing field images computed by Equation (10) are shown

in Figure 12 for both TE and TM case. To clearly observe the 90 degree phase difference between the real and the imaginary part of a propagating wave field in the waveguide we plot the real part on the upper halves and the imaginary part on the button halves. No information is lost due to the even symmetry (toward $z$-axis) of the
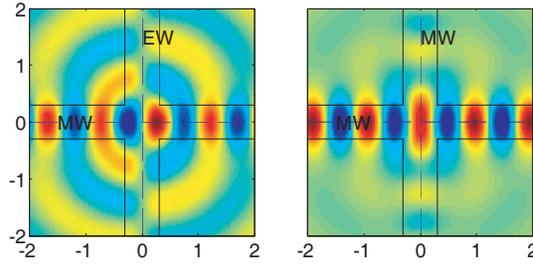


**Figure 13.** Expanded $E_y(x, z)$ field distributions of the plus-symmetry model for the dielectric waveguide crossing. The wavelength is $1.3\,\mu\mathrm{m}$. The core index is 1.5 and the cladding index is 1. The core thickness is $0.6\,\mu\mathrm{m}$. The thin blue dashed lines are the symmetry axes and the core-cladding boundaries are marked by thin dark lines.
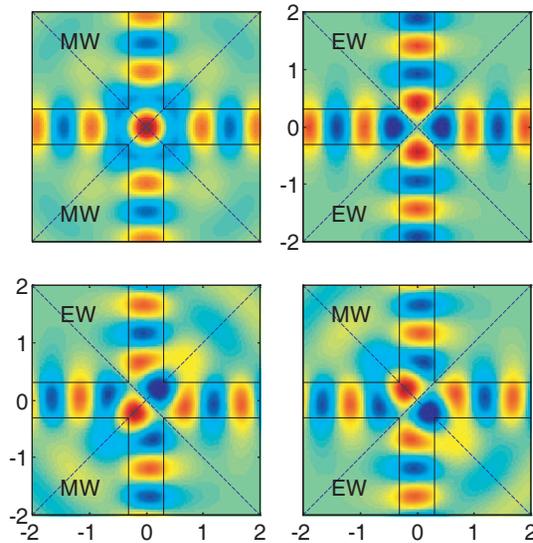


**Figure 14.** Expanded $E_y(x, z)$ field distributions of the cross-symmetry model for the dielectric waveguide crossing. The parameters are same as those in Figure 13.
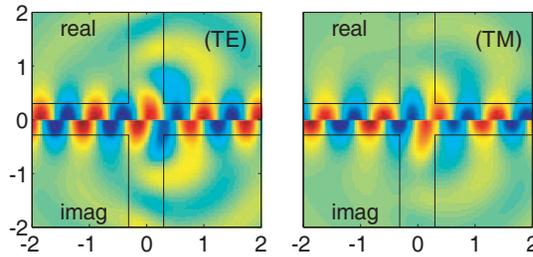
**Figure 15.** TE and TM field distributions of an open dielectric slab waveguide constructed from averages of Figures 13–14. These complex EM fields are shown with the real part on the upper halves and the imaginary part on the bottom halves.

crossing wave fields. To check our result, we re-compute the same field with the cross-symmetry mode. The four expanded full fields are shown in Figure 12. The figures provide us with a direct validation of Equations (12)–(13) in handling the FD coefficients for points on the cross symmetry axes. We report that for averaged absolute relative difference between the plus and cross model is less than 0.1% for this waveguide configuration.

Figures 13–14 show the field distribution of a dielectric waveguide crossing computed with the plus- and cross-symmetry model for the TE mode respectively. The open dielectric slab waveguide is air-clad with a 1.5 core index and a core thickness of 0.6 micron operated at a wavelength of 1.3 micron. The complete field solution of a dielectric crossing waveguide is shown in Figure 15 for both TE and TM polarization.

## 4.2. Universal and Quasi-universal Curves for the Power Coupling Coefficients

With the hybrid FD-FD simulation of crossing waveguides, we are able to obtain mode-to-mode through and cross coupling coefficients as well as reflection coefficients as function of wavelength and waveguide structure parameters. In Figures 16–17, we plot total power transfer coefficients against the normalized frequency for microwave crossing waveguides for both the plus and cross-symmetry models. Here $P_r$ is the total reflected power coefficient $P_t$ is the total through-transmission coefficient and $P_v$ is the total cross-transmission coefficient for the upper and lower waveguides combined. We denote the sum of $P_r$, $P_t$, $P_v$ as $P_s$ which represents the total scattered power coefficient
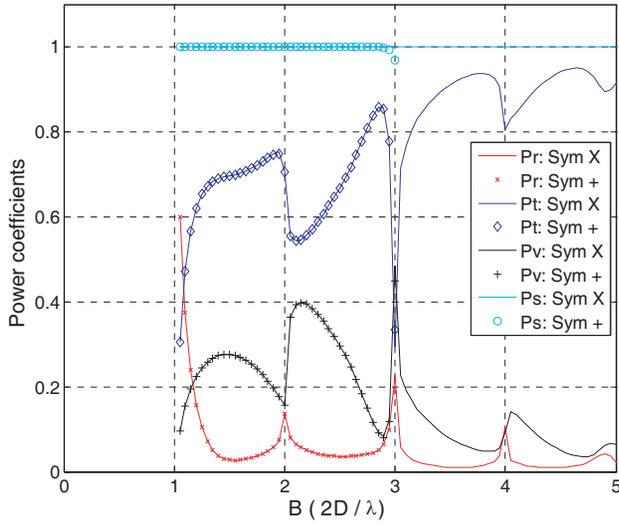
**Figure 16.** Total power transfer coefficients for the TE mode microwave crossing waveguide. Data are computed with both the plus- and the cross-symmetry models Note that TE mode is cutoff for $B$ less than 1.
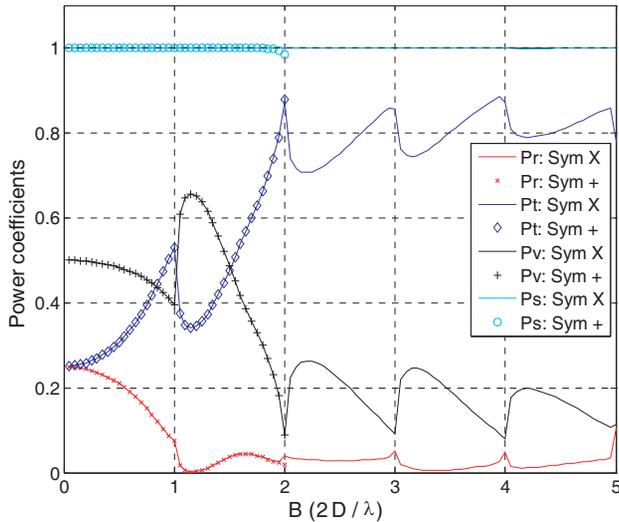


**Figure 17.** Same as in Figure 16 except for the TM polarization.

due to an incident mode field. In a lossless waveguide $P_s$ is always one. It is plotted in Figures 16–17 to verify the power conservation in our Matlab codes For these microwave cases, we have power conservation accurate to the fourth decimal place. The results for the plus and the crosssymmetry cases agree with each other for the $B$ parameter ranges from 1 to 3. However, we find increasing error for the plus-symmetry cases after $B > 3$. Starting from $B = 3$, we have additional guiding mode and the single-guiding-mode TBC approximation for the upper boundary is not valid anymore. Thus, we show only the cross-symmetry model data beyond that point.
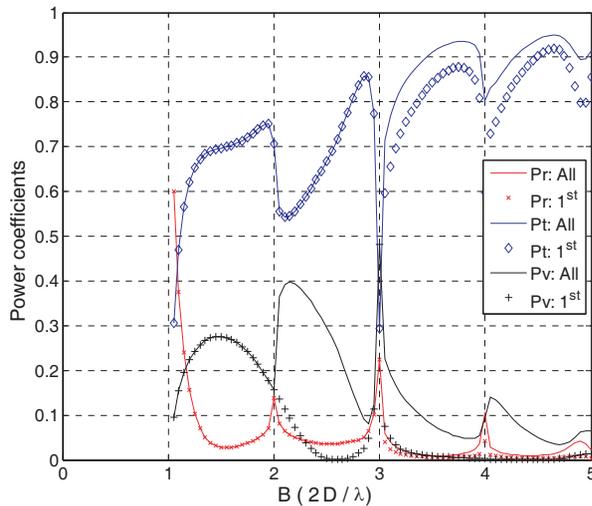


**Figure 18.** TE mode, total and fundamental-mode, reflected, cross and through power coupling coefficients as function of normalized frequency.

In Figures 18–19, we plot fundamental-mode power coupling coefficients (reflected, cross and through) for TE and TM modes computed with the cross-symmetry model. From the numerical results, part of the power is transferred from the fundamental mode to the other higher-order modes including the radiation modes. In particular, the upward and downward powers of the fundamental guiding mode are quite small and fields are dominated by higher-order guiding modes and radiation modes.

The normalized frequency of a dielectric slab waveguide with a full core thickness $D$ and core/cladding indices of $n_{\mathrm{cor}}, n_{\mathrm{cld}}$ is defined as

$$V = \sqrt{n_{\mathrm{cor}}^2 - n_{\mathrm{cld}}^2}\, \frac{2\pi}{\lambda} D. \tag{16}$$
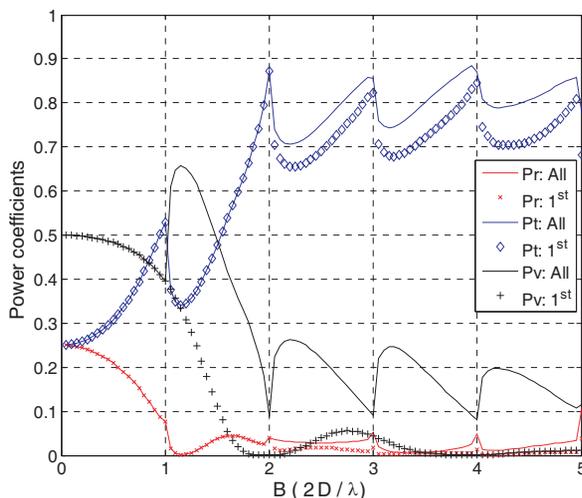
**Figure 19.** Same as Figure 18 except for TM polarization.
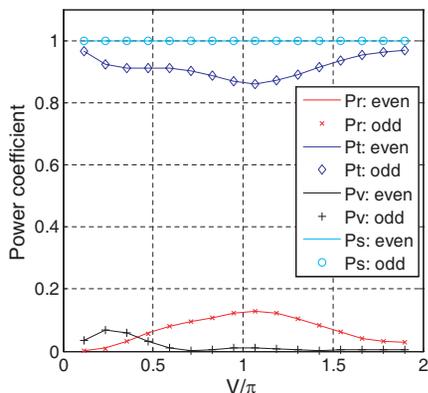


**Figure 20.** Total reflected, cross and through power coupling coefficients of the dielectric crossing waveguide versus core thickness expressed in the normalized frequency for TE case. Data are computed with both even and odd $N_x$ grids. The fixed parameters are $\lambda = 1.3\,\mu\text{m}$, $n_{cor} = 1.5$ and $n_{cld} = 1$.
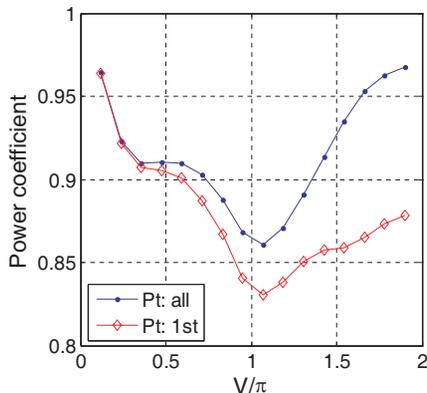
**Figure 21.** Total and fundamental-mode through power coupling coefficients versus waveguide core width expressed in the normalized frequency for TE case. Waveguide parameters are given in Figure 20.

This normalized frequency uniquely determines the number of guided modes in a dielectric slab waveguide but exact mode field profiles depend on values of $n_{cor}, n_{cld}$ as well as its core thickness. There are no universal curves for the dielectric crossing waveguide even though $V$ is still the most important parameter for such curves. Thus, quasi-universal curves for power coupling coefficients of the dielectric crossing waveguide are plotted in Figures 20–25 as functions of $V/\pi$, the dielectric equivalent to the microwave normalized frequency $B$ of Equation (15).

These data are computed with just the cross model since the fundamental-mode approximation used in the plus model produces noticeable errors. Therefore, for numerical verification we compute results with both the even and the odd $N_x$ formulation. Our numerical results in Figures 20 and 23 indicate that differences between even and odd $N_x$ grids are in the order of $10^{-4}$ or less.

In Figure 24 of the TM case, we find the minimum insertion loss for an air-clad glass slab waveguide, occurs at $V/\pi = 0.7127$, is about $0.11\,\mathrm{dB}$ (97.6% power transmission coefficient for the fundamental mode). At this point the cross talk is $-28.0\,\mathrm{dB}$. However, for the TE case in Figure 21 the corresponding insertion loss increases to $0.52\,\mathrm{dB}$ (88.7%) for the fundamental mode and the cross-talk is $-26.4\,\mathrm{dB}$. For
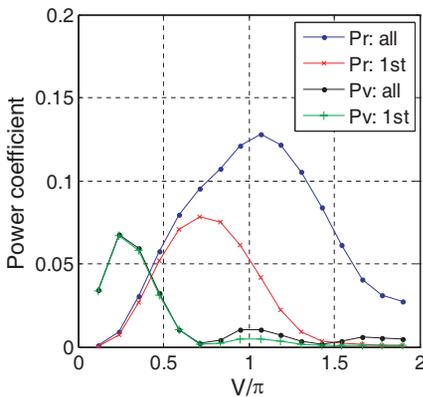


**Figure 22.** Total and fundamental-mode reflected and cross power coupling coefficients versus waveguide core width expressed in the normalized frequency for TE case. Waveguide parameters are given in Figure 20.
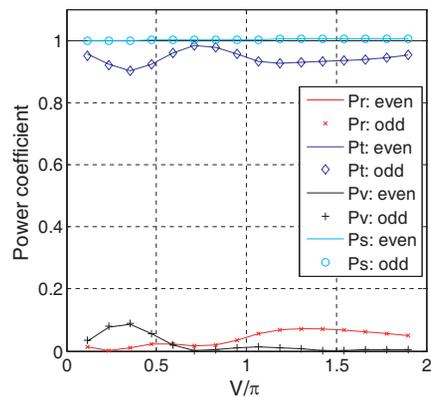
**Figure 23.** Total reflected, cross and through power coupling coefficients for TM polarization See Figure 20 for waveguide parameters.
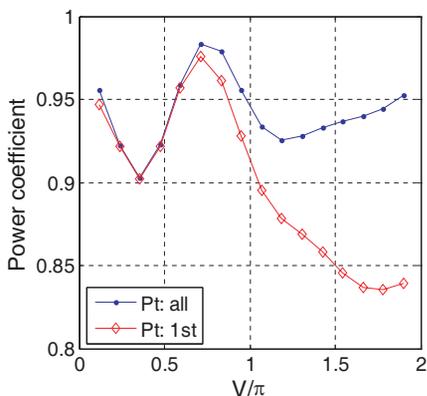
**Figure 24.** Total and fundamental-mode through power coupling coefficients for TM polarization. See Figure 20 for waveguide parameters.
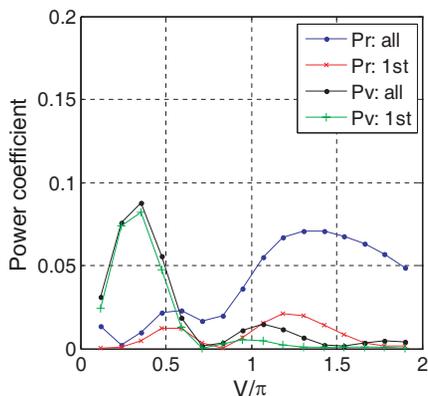
**Figure 25.** Total and fundamental-mode reflected and cross power coupling coefficients for TM polarization. See Figure 20 for waveguide parameters.

the TE mode, the minimum insertion loss is at the beginning of the $V$ parameter which corresponds to a very small core width. Thus, insertion loss for the dielectric crossing waveguide is highly polarization dependent as well as highly sensitive to the waveguide parameters.

## 5. CONCLUSIONS

We proposed a hybrid frequency-domain finite difference method to study the microwave and the open dielectric crossing waveguide for both TE and TM modes by exploiting built-in dual structural symmetries in these devices. The plus and cross symmetry models not only simplify the implementation of the layer-mode based transparent boundary conditions but also reduce much required computational resources. Our numerical data are verified by cross-checking results from two symmetry models and from using even and odd $N_x$ grids for the cross model. Finally, FD-FD results are shown with field images and normalization curves for the reflected, cross and through power coupling coefficients of the crossing waveguide.

## ACKNOWLEDGMENT

## REFERENCES

1. Gaburro, Z., *Silicon Photonics*, Ch. 4, Optical Interconnect, Topics in Appl. Phys., Vol. 94, 121–176, 2004.

2. Pavesi, L. and G. Guillot, *Optical Interconnect*, Springer-Verlag, Berlin, Heidelberg, 2006.

3. Beausoleil, R. G., P. J. Kuekes, G. S. Snider, S.-Y. Wang, and R. S. Williams, "Nanoelectronic and nanophotonic interconnect," *Proc. IEEE*, Vol. 96, 230–247, 2008.

4. Daly, M. G., P. E. Jessop, and D. Yevick, "Crosstalk reduction in intersecting rib waveguide," *Journal of Lightwave Technology*, Vol. 14, 1695–1698, 1996.

5. Johnson, S. G., C. Manolatou, J. D. Joannopoulos, et al., "Elimination of cross talk in waveguide intersections," *Optics Letters*, Vol. 23, 1855–1857, 1998.

6. Manolatou, C., S. G. Johnson, J. D. Joannopoulos, et al., "High-density integrated optics," *Journal of Lightwave Technology*, Vol. 17, 1682–1692, 1999.

7. Fukazawa, T., T. Hirano, F. Ohno, and T. Baba, "Low loss intersection of Si photonic wire waveguides," *Jpn. J. Appl. Phys.* Vol. 43, 646–647, 2004

8. Liu, H., H. Tam, P. K. A. Wai, and E. Pun, "Low-loss waveguide crossing using a multimode interference structure," *Optics Communications*, Vol. 241, 99–104, 2004.

9. Jamid, H. A., M. Z. M. Khan, and M. Ameeruddin, "A compact 90° three-branch beam splitter based on resonant coupling," *Journal of Lightwave Technology*, Vol. 23, 3900–3906, 2005.

10. Chen, H. and A. W. Poon, "Low loss multimode interference based crossings for silicon wire waveguides," *IEEE Photonics Tech. Letters*, Vol. 18, No. 21, 2260–2262, 2006.

11. Bogaerts, W., P. Dumon, D. V. Thourhout, and R. Baets, "Low-loss, low-cross-talk crossings for silicon-on-insulator nanophotonic waveguides," *Optics Letters*, Vol. 32, 2801–2803, 2007.

12. Sanchis, P., J. V. Galn, A. Griol, J. Mart, M. A. Piqueras, and

J. M. Perdigues, "Low-crosstalk in silicon-on insulator waveguide crossings with optimized-angle," *IEEE Photon. Technol. Lett.*, Vol. 19, 1583–1585, 2007.

13. Menzel, W. and I. Wolff, "A method for calculating the frequency-dependent properties of microstrip discontinuities," *IEEE Transactions on Microwave Theory and Techniques*, Vol. 25, 107–112, 1977.

14. Li, J., D. A. Fattal, and R. G. Beausoleil, "Crosstalk-free design for the intersection of two dielectric waveguides," *Optics Express*, Vol. 17, 7717–7724, 2009.

15. Neyer, A., W. Nevenkamp, L. Thylen, and B. Lagerstrom, "A beam propagation method analysis of active and passive waveguide crossings," *Journal of Lightwave Technology*, Vol. 3, 635–642, 1985.

16. Hammer, M., "Hybrid analytical/numerical coupled-mode modeling of guided-wave devices," *Journal of Lightwave Technology*, Vol. 25, 2287–2298, 2007.

17. Chang, H. W., Y. H. Wu, S. M. Lu, and W. C. Cheng, "Field analysis of dielectric waveguide devices based on coupled transverse-mode integral equation — Numerical investigation," *Progress In Electromagnetics Research*, PIER 97, 159–176, 2009.

18. Chang, H.-W. and M.-H. Sheng, "Field analysis of dielectric waveguide devices based on coupled transverse-mode integral equation — Mathematical and numerical formulations" *Progress In Electromagnetics Research*, PIER 78, 329–347, 2008.

19. Borges, B.-H. V. and P. R. Herczfeld, "Coupled-mode analysis of highly asymmetric directional couples with periodic perturbation," *IEEE Trans. Microwave Theory Tech.*, Vol. 46, No. 3, 215–226, 1998.

20. Hammer, M., "Quadridirectional eigenmode expansion scheme for 2-D modeling of wave propagation in integrated optics," *Optics Communications*, Vol. 235, 285–303, 2004.

21. Mittra, R. and U. Pekel, "A new look at the perfectly matched layer (PML) concept for the reflectionless absorption of electromagnetic waves," *IEEE Microwave and Guided Wave Letter*, Vol. 5, No. 3, 84–86, 1995.

22. Moerloose, J. D. and M. A. Stuchly, "Behavior of Berenger's ABC for evanescent waves," *IEEE Microwave and Guided Wave Letter*, Vol. 5, No. 10, 344–346, 1995.

23. Cheng, W.-C. and H.-W. Chang, "Comparison of PML with layer-mode based TBC for FD-FD method in a layered medium,"

*International Conference on Optics and Photonics in Taiwan*, P1-170, Dec. 2008.

24. Chang, H. W., W.-C. Cheng, and S.-M. Lu, "Layer-mode transparent boundary condition for the hybrid FD-FD method," *Progress In Electromagnetics Research*, PIER 94, 175–195, 2009.

25. Chang, H. W., "FD-FD analysis of dielectric waveguide crossings with two-fold symmetry," *The XVIIIth International Workshop on Optical Waveguide Theory and Numerical Modeling*, Session 4, 21, 2009.

26. Cheng, W.-C., "Finite-different frequency-domain analysis of a dielectric waveguide crossing," Ph.D. Thesis, Department of Photonics, National Sun Yat-sen University, 2010.

27. Chang, H.-W. and S.-M. Wang, "Large-scale hybrid FD-FD method for micro-ring cavities," *FWE6 Frontier in Optics*, 2005.